Article

Mesoscale Analysis of Rubber Particle Effect on Indirect Tensile and Flexural Tensile Strength of Crumb Rubber Mortar

Huailiang Chen [1,2], Danda Li [1], Xing Ma [1,*], Zheng Zhong [3] and El-Sayed Abd-Elaal [1,4]

1. UniSA STEM, University of South Australia, Adelaide, SA 5065, Australia
2. School of Civil Engineering, Jiangsu College of Engineering and Technology, Nantong 226006, China
3. School of Science, Harbin Institute of Technology, Shenzhen 518055, China
4. Department of Structural Engineering, Mansoura University, Mansoura 35516, Egypt
* Correspondence: xing.ma@unisa.edu.au

Abstract: This paper presents a mesoscale model to study the influence of rubber particles on the mechanical performance of crumb rubber mortar (CRM). The indirect tensile and flexural behaviors of CRM with different rubber replacement rates, shapes, and sizes were investigated. Rubber mortar is assumed to be a three-phase material composed of rubber aggregate, a mortar matrix, and an interface transition zone (ITZ). Numerical analysis showed that rubber content was the governing factor affecting the reduction rate of indirect tensile and flexural strength. The effect of the ITZ on the tensile strength of CRM was within one percent, which could be ignored. The influence of rubber particle size was investigated by analyzing CRM models containing five different rubber sizes from 0.86 mm to 7 mm. For each size, six different models with randomly distributed rubber particles were set up. CRM models presented a similar average strength even with different rubber particle sizes. However, the strength variation among the random models became higher when the rubber particle size increased. Numerical results also proved that treating rubber particles as pores in modeling led to negligible errors. Then, a prediction formula after considering the increase in air content is provided. Finally, the accuracy of numerical simulations was verified through a series of experimental studies.

Keywords: crumb rubber mortar (CRM); flexural tensile strength; indirect tensile strength; mesoscale analysis

1. Introduction

The issue of how to reduce dependency on natural aggregates in the production of concrete products and mortars has always been a concern in the construction industry. The use of crumb rubber to partially substitute fine aggregates in concrete products can consume less non-renewable natural resources and offer an alternative option to the disposal of recycled tire rubber in an eco-friendly way. The use of crumb rubber in Portland cement concrete products mainly includes lightweight concrete, foam concrete, and cement mortar. Scholars have studied the application of CRM (crumb rubber mortar) in wall coatings [1], geopolymer mortar [2], masonry mortars [3], render mortars [4], pavements [5], self-consolidating mortars [6], and lightweight-foamed CRM [7], as well as its application as a filler material in structural composite walls [8–10]. The existing literature on CRM is mainly focused on the influence of the addition of rubber particles on the mechanical and physical properties of CRM, indicating that the addition of rubber particles results in a significant decrease in the strength of the rubber mortar. Researchers have performed a lot of work to explore the factors that affect the mechanical behaviors of CRM. Wongsa et al. (2018) replaced 100% of natural sand in geopolymer mortar with crumb rubber. The results showed that the compressive strength was reduced by 93%, and the flexural strength was reduced by 74% [2]. However, the compressive strength of the crumb rubber geopolymer mortar could still reach 2.07–3.29 MPa, which was still suitable for non-load-bearing bricks.

Marques et al. (2008) studied the mechanical strength of mortar mixed with crumb rubber at a level of 12% by volume. The compressive strength and splitting tensile strength of the CRM at 28 days were 40% and 37% lower than those of the control mortar, respectively [11]. Uygunoğlu and Topçu (2010) reported that the rubber content and the water–cement ratio affected the compressive strength of CRM. The compressive strength decreased with increasing rubber content and water–cement ratio. The flexural strength also decreased with the increase in rubber content [6]. Correia et al. (2010) produced CRM specimens with rubber substitution levels at 10%, 20%, and 30% and with water–cement ratios of 0.52, 0.55, and 0.60. Their experiment results concluded that for the specimens with three types of rubber content, the greater the water–cement ratio, the lower the compressive strength [12]. Song et al. (2018) prepared CRM samples with rubber contents of 5%, 10%, 15%, and 20% by weight and tested the stress–strain curves of CRM under triaxial stress. The results indicated that the compressive strength reduced as the rubber content increased. For samples with the same content of rubber particles, increasing the confining pressure could increase their compressive strength [13]. Yu and Zhu (2016) prepared CRM samples containing rubber particles with sizes of 2–4 mm, 1–3 mm, and 0–2 mm and with contents of 17%, 33%, and 50% by volume [14]. The results indicated that the CRM with smaller-sized rubber had a higher total pore volume. The low stiffness of the rubber particles and the large pores in the sample were the main reasons for the decrease in strength.

Experimental tests were conducted to study the effect of rubber particle size on the mechanical performance and pore structure characteristics of CRM. The studies showed that the total pore volume in CRM increased with increasing rubber content. The compressive strength, flexural strength, splitting strength, and elastic modulus of CRM were significantly reduced with an increase in rubber content. The strength reduction in the CRM was attributed to the lower stiffness and the increase in porosity due to the incorporation of rubber particles. In addition to this reason, two other potential aspects weakened the mechanical strength of CRM. The first reason was the weak bond between rubber particles and the mortar matrix [15]. The second reason was that voids were observed between the rubber particles and the mortar matrix, which would increase the porosity of the interface transition zone [16]. In general, it was well accepted that the strength of the CRM was reduced when compared with the control mortar. The strength reduction rates might be affected by the rubber content, rubber particle size, and/or the bonding strength on the interfaces between the rubber particles and mortar.

The coefficient of thermal expansion, elastic modulus, strength, and deformability of rubber particles are quite different from that of the mortar matrix in CRM. The incorporation of crushed rubber particles into the mortar mixture changes the internal structure of the rubber mortar, such as increasing the porosity of the mortar matrix, especially the interface layer. The mechanical properties of CRM may be more unstable and difficult to predict through experiments compared with normal mortar. A potential numerical model is introduced to reconstruct the internal composition of CRM and evaluate the effect of rubber particles on its mechanical performance. Studying the effect of rubber particles on the tensile strength of cement mortar is an integral part of evaluating its mechanical properties, and it is also a reference for evaluating its resistance to thermal cracking and shrinkage cracking.

Two- and three-dimensional mesoscale models have been developed to study the mechanical properties of conventional concrete under static direct tension [17,18], static compression [19–21], dynamic direct tension [22], and dynamic compression [23,24]. Existing work on rubberized concrete is relatively limited compared to normal concrete. Duarte et al. (2015) and Duarte et al. (2017) conducted a 2D mesoscale simulation to study the mechanical behavior of rubber concrete under compressive and indirect tensile loadings [25,26]. Li et al. (2019) and Diao et al. (2020) proposed a 3D mesoscale model to analyze the uniaxial tensile strength of self-compacting rubberized concrete [27,28]. To the best of the authors' knowledge, no mesoscale analysis of rubber mortar has been found in the existing literature.

The above literature shows that the addition of rubber reduces the strength of CRM. However, the rate of strength reduction varies greatly in different studies [7–14]. The existing work is mainly based on experimental study through qualitatively describing the reasons for strength reduction. To date, there is still no quantitative analysis to expose the fundamental mechanism of the strength reduction in CRM in terms of rubber particle parameters. Numerical analysis is an effective method to fill this research gap. In this paper, a mesoscale model is first employed to study the rubber particle effect on the indirect tensile and flexural strengths of CRM. The influence of rubber content, size, distribution, interface layer, mortar matrix strength, and treating rubber particles as pores on the indirect tensile strength of CRM is studied. A general formula for predicting the indirect tensile and flexural strength of CRM is also developed.

In the numerical simulation, the distribution of crumb rubber granules in the three-dimensional specimen was transformed into a plane model using the Walraven equation. CRM is regarded as a three-phase material: rubber particles, mortar matrix, and interface layer. Circles and circle-derived polygons are used to consider the influence of regular and irregular shapes.

2. Experiment Program

2.1. Mix Proportions Design

Two to four mm of untreated rubber granules (Figure 1) were used to replace 6%, 12%, and 18% of the volume of fine aggregate in ordinary mortar, respectively. Table 1 lists the amount of each material in the three types of CRM samples. The relative density of sand, rubber particles, and cement in Table 1 is 2630 kg/m^3, 1140 kg/m^3, and 3150 kg/m^3, respectively.

Figure 1. 2–4 mm rubber granules.

Table 1. Mix proportions of CRM.

Mix	Rubber Content (%)	Cement (kg/m^3)	Sand (kg/m^3)	Water (kg/m^3)	Rubber (kg/m^3)
Control	0.00%	678.0	1164.4	339.0	0.0
CRM6	6.00%	678.0	1094.5	339.0	30.3
CRM12	12.00%	678.0	1024.7	339.0	60.6
CRM18	18.00%	678.0	954.8	339.0	90.9

2.2. Specimen Preparation and Test Program

According to AS 1012.8.1 (2014), cylindrical rubber mortar specimens with a diameter of 100 mm and a height of 200 mm were cast for the indirect tensile strength test [29]. ASTM: C-348-20 (1999) was followed to prepare rubber mortar prisms with a size of 40 × 40 × 160 mm for the flexural strength test [30]. Twenty-four hours after pouring was completed, the mold was removed from the specimen, and the specimens were placed in the curing room for 28 days. Six specimens were poured for each rubber mortar mixture.

Following the procedure in AS 1012.10 (2000), the indirect tensile test was carried out using an automatic concrete compression testing machine to apply the load at a rate of 0.8 kN/s (Figure 2) [31]. The testing machine was made by CONTROLS Inc. based in Tucker GA, 30084, United States. Under the requirements of ASTM: C-348-20 (1999), the Instron Universal Testing machine was used to perform a three-point flexural test with a loading rate of 0.5 cm/min (Figure 3) [30]. The instrument was made by Instron Engineering Corporation based in Canton, MA, USA. The specimen was simply supported on the testing machine.

Figure 2. Indirect tensile test setup.

Figure 3. Three-point flexural test setup.

3. Mesoscale Simulation of Crumb Rubber Mortar

The mesoscale analysis is an effective method to study the properties of cementitious materials when the inhomogeneity of their internal structure needs to be considered. CRM is a composite material with an uneven internal structure, and its failure process and mode are closely related to the properties of its constituent materials. This section briefly introduces how to generate a mesoscale model of CRM and analyzes the influence of rubber particle parameters on the tensile strength of CRM using this model.

3.1. Mesoscale Model Formation of Rubber Mortar

3.1.1. Conversion of the Distribution of Rubber Particles from Space to a Plane

Chen et al. (2021) introduced the procedure of using the Walraven equation to convert the content of rubber particles in a 3D crumb rubber concrete sample to the content on a plane [32]. Similarly, the content of rubber particles on a 2D rubber mortar specimen can also be obtained using the methods they provide, which mainly include three steps. The sand in each size range is assumed to satisfy W.B. Fuller's grading curve. The first step is to obtain the 3D grade curve of the sand. The size of natural sand in Table 1 is assumed to be in the range of 0.5–5 mm, which is further divided into three ranges of 5–4 mm, 4–2 mm, and 2–0.5 mm to calculate the 3D grading cure of the sand. The equation of W.B. Fuller's grading curve is used to calculate the volume content of sand in each size range, as shown in Table 2. Figure 4 compares the 3D and 2D gradation curves of the sand with three size ranges. The last step is to determine the rubber content in the 2D state using Equation (1). The results of CRM with five rubber contents are shown in Table 3.

$$A_R = \frac{P_k \times R_p \times A_s}{V_s} \tag{1}$$

where A_R is the area ratio of rubber particles with a size of 2–4 mm to the cross-section of the specimen. P_k is the ratio of total sand volume to specimen volume, equal to 44.27%. R_p is the volume replacement rate, and the value in this paper is 6~18%. A_s is the area ratio of sand with a size of 2–4 mm to the cross-section of the specimen. V_s is the volume ratio of sand with a size of 2–4 mm to the specimen.

Table 2. 3D gradation and 2D design of sand in the control mortar.

Mix	Type of Aggregate	Size Range (mm)	3D $V_s[d_s,d_{s+1}]$	2D $A_s[d_s,d_{s+1}]$
Control mortar	sand	0.5–2	6.84%	3.13%
		2–4	16.96%	11.29%
		4–5	20.47%	14.85%

$V_s[d_s,d_{s+1}]$, the volume ratio of sand with a single size range to the specimen. $A_s[d_s,d_{s+1}]$, the area ratio of sand with a single size range to the cross-section of the specimen.
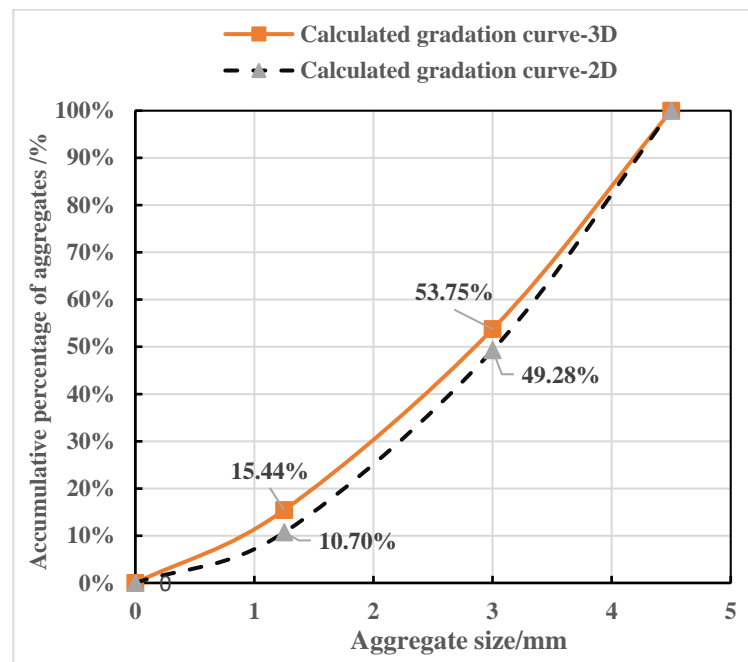

Figure 4. 3D and 2D gradation curves of sand and its three size ranges.

Table 3. 3D gradation and 2D design of crumb rubber particles in CRM mortar.

Mix	Type of Aggregate	Size Range (mm)	3D V_R [2,4]	2D A_R [2,4]
CRM6			2.66%	1.77%
CRM12	Crumb rubber granules	2–4	5.31%	3.54%
CRM18			7.97%	5.31%

V_R [2,4], the volume ratio of rubber particles with a size of 2–4 mm to the specimen. A_R [2,4], the area ratio of rubber particles with a size of 2–4 mm to the cross-section of the specimen.

3.1.2. Simulation of the Shape of Rubber Particles and Their Interface Layer

In two-dimensional mesoscale finite element modeling, circles, ellipses, and random polygons are widely used to simulate the shape of coarse aggregates in normal concrete [33]. In this study, circles and circle-derived polygons are adopted to simulate the shape of rubber particles. The thickness of the ITZ between cement and coarse aggregate in conventional concrete is around 15–50 μm [34]. However, the thickness of the interface layer between the rubber particles and the mortar matrix in rubber concrete or rubber mortar is not found in the available published work. In this study, the thickness of the ITZ in CRM is assumed to be similar to that of ordinary concrete. The thickness of the ITZ is set to 0.05 mm to study its effect on the tensile strength of CRM. Take the circle-derived hexagonal rubber particle as an example to describe how to generate random polygonal rubber particles with six vertexes (Figure 5). Assuming that the diameter of the rubber particles is d, draw the first circle marked "Circle-1". The six points marked "1"~"6" (Figure 5) are used to equally divide the circumference of "Circle-1". The first vertex marked "A" is randomly selected between point "1" and point "6", and the other five vertexes are chosen similarly. The six vertexes marked "A"~"F" are used to connect a sequence to form a random hexagon, and this polygon is offset by 0.05 mm to the outside to obtain the second polygon. The shaded area between these two polygons is the interface layer of the rubber particles in the CRM, as shown in Figure 5. The number of the sides of the random polygons used in this study is set to 4~10, which can be created similarly. In addition to the creation of circular and random circle-derived polygonal particles, other main tasks mainly include determining the random position of aggregates and realizing non-contact between the aggregates, which are provided in [32].
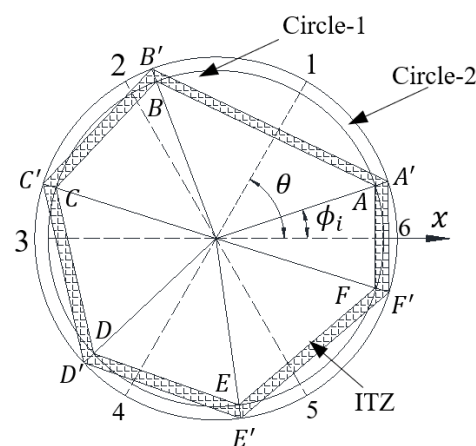

Figure 5. A hexagonal rubber particle and its interface layer.

3.1.3. Mesoscale Models of CRM Specimens

Based on the algorithm for creating aggregates and interface layers, a code was developed to place rubber particles within the boundaries of the 2D specimen and obtain the parameters of circles and polygons required by ABAQUS to create circles and polygons. The parameters were imported into ABAQUS to create 2D mesoscale models of CRM containing three rubber contents listed in Table 1. Figure 6 shows the circular CRM sample

with a diameter of 100 mm used in the model. The 40 × 160 mm specimen for the three-point flexural strength model is shown in Figure 7. The finite element software version used in this study is ABAQUS2018, purchased by UniSA.
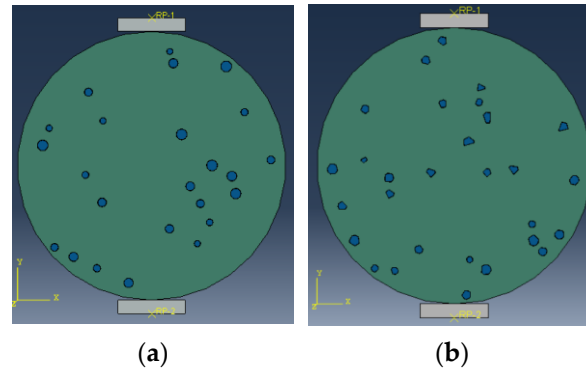

(a)   (b)

Figure 6. CRM specimens for indirect tensile test. (**a**) CRM 6 with circular rubber particles. (**b**) CRM 6 with circle-derived polygonal rubber particles.
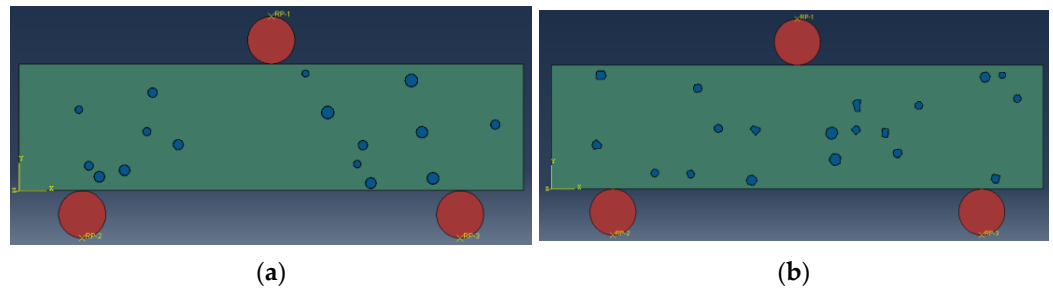

(a)   (b)

Figure 7. CRM specimens for three-point flexural test. (**a**) CRM 6 with circular rubber particles. (**b**) CRM 6 with circle-derived polygonal rubber particles.

3.1.4. Mechanical Properties of Three-Phase Materials in Rubber Mortar

In the mesoscale analysis of rubber mortar, the rubber particles are regarded as elastic materials, and the mortar matrix and its interface layer with rubber particles are treated as elastoplastic materials, which will crack under the action of external force. The interface between the rubber particles and the mortar matrix, also called the ITZ, is regarded as a material like mortar, but with reduced strength. Since mortar is also a quasi-brittle material, its stress–strain behavior can be simulated with the concrete damage plastic model (CDP) provided by ABAQUS. The tensile damage parameters d_t and compressive parameters d_c need to be determined first and input into the material properties of the CDP model.

Equations (2) and (3) can be used to describe the stress–strain behavior of concrete under uniaxial tension and compression loads, respectively [35].

$$\sigma_t = (1 - d_t)E_0\left(\varepsilon_t - \widetilde{\varepsilon}_t^{pl}\right) \tag{2}$$

$$\sigma_c = (1 - d_c)E_0\left(\varepsilon_c - \widetilde{\varepsilon}_c^{pl}\right) \tag{3}$$

where d_t and d_c are tensile and compressive damage variables, respectively. E_0 is the elastic modulus of the material. $\widetilde{\varepsilon}_t^{pl}$ and $\widetilde{\varepsilon}_c^{pl}$ are the equivalent tensile and compressive plastic strains of the material, respectively.

The tensile and compressive damage parameters were calculated using the method proposed by Birtel and Mark (2006) [36]. This method assumes that the plastic strain is a

certain proportion of cracking strain. The cracking strain is calculated by subtracting the elastic strain from the total strain using Equation (4):

$$\widetilde{\varepsilon}_t^{ck} = \varepsilon_t - \frac{\sigma_t}{E_0} \tag{4}$$

where $\widetilde{\varepsilon}_t^{ck}$ is the cracking strain, ε_t is the total strain, σ_t is the tensile stress, and E_0 is the initial elastic modulus of the material.

Set a constant factor η_t with $0 < \eta_t \leq 1$, $\widetilde{\varepsilon}_t^{pl} = \eta_t \times \widetilde{\varepsilon}_t^{ck}$, and substitute Equation (4) into Equation (2) to obtain the Equation (5) that can determine the value of d_t. Similarly, the compressive damage parameter d_c is determined using Equation (6):

$$d_t = \frac{E_0 \times \widetilde{\varepsilon}_t^{ck} \times (1 - \eta_t)}{\sigma_t + E_0 \times \widetilde{\varepsilon}_t^{ck} \times (1 - \eta_t)} \tag{5}$$

$$d_c = \frac{E_0 \times \widetilde{\varepsilon}_c^{in} \times (1 - \eta_c)}{\sigma_c + E_0 \times \widetilde{\varepsilon}_c^{in} \times (1 - \eta_c)} \tag{6}$$

where $\widetilde{\varepsilon}_c^{in}$ is the inelastic strain of the material, η_c is a constant factor with $0 < \eta_c \leq 1$, and σ_c is the compressive stress of the material.

The uniaxial compressive stress–strain curve was estimated from experimental tests using the average from three mortar samples poured with the controlled mix ratio as given in Table 1. A linear variable differential transformer was installed on the specimen to measure and record the vertical displacement in the compression test (Figure 8). The four points in the ascending section and the two points in the descending section are selected as the representative points of the stress–strain curve of each specimen. The average value of the three specimens was calculated to draw the stress–strain curve of normal mortar, as shown in Figure 9. The six points in the curve marked as the "average of three specimens" were substituted into Equation (6) to calculate the compression damage parameters.

Figure 8. Test device for measuring the compressive stress–strain curve of control mortar.

In this paper, only the tensile strength of ordinary mortar was recorded in the indirect tensile test. Since the direct tensile stress–strain test of mortar is difficult to be measured experimentally, this article assumes that the relationship between stress and strain is linear with a drop after point 4, similar to the compression test in Figure 9. Then, the tensile damage parameters were determined using Equation (5) similarly.
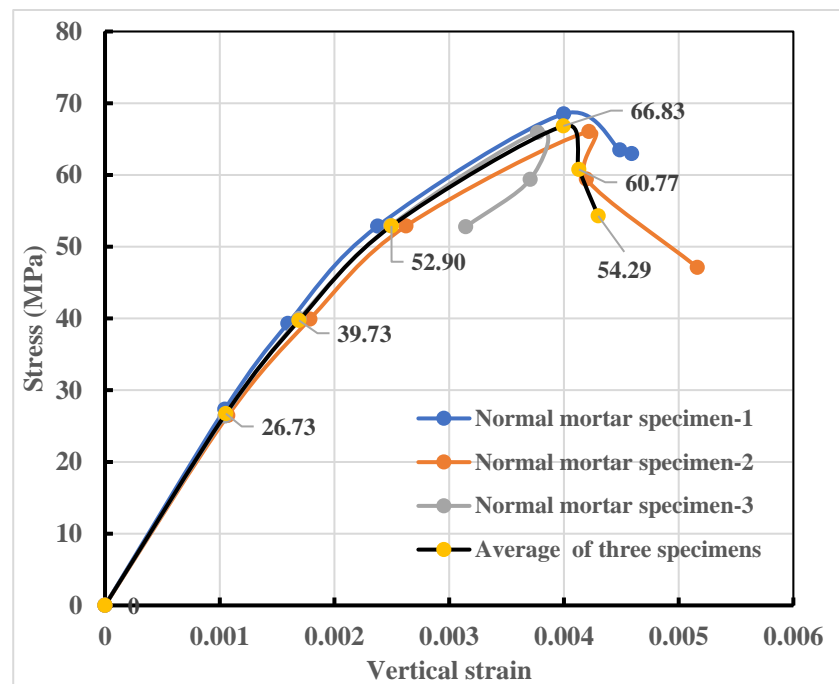
Figure 9. The uniaxial compressive stress–strain curve of the control mix.

Wang et al. (2020) studied the microporous structure of the ITZ in crumb rubber concrete. The results showed that there were more pores and line-like microcracks around rubber particles than stones. The hydrophobicity of the rubber results in weak connections between the rubber particles and the mortar. When the rubber particles were pulled from the section of the sample, there were almost no hydration products on the surface of the rubber particles [37]. An interface layer with a thickness of 0.05 mm is intentionally inserted around the boundary of each rubber particle to simulate the ITZ of the rubber mortar. The compressive strength and tensile strength of the ITZ were first assumed to be equal to the mortar matrix. Then, the impact of changing the strength of the ITZ on the overall tensile strength of CRM was also studied. The micro-nano indentation test shows that Young's modulus and the strength of the ITZ are around 60–85% of the mortar phase in ordinary concrete and recycled aggregate concrete [38,39]. In this paper, Young's modulus and the strength of the ITZ were 60% of the mortar phase. Table 4 lists the parameters of the three components of the CRM.

Table 4. Material properties.

Composition	Young's Modulus (MPa)	Poisson's Ratio	Compressive Strength (MPa)	Tensile Strength (MPa)
Mortar	25,374.26	0.2	66.83	3.98
Rubber particles *	3	0.49		
ITZ	25,374.26 * 60%	0.2	66.83 * 60%	3.98 * 60%

Note: * refers to the data adapted with permission from Ref. [25], Duarte et al. (2015).

3.1.5. Simulation of Indirect Tensile Test

The numerical simulation of the indirect tensile test has been conducted on a 2D specimen, as shown in Figure 10. Two wood-bearing strips with a size of 25 × 5 mm are modeled and placed on the top and bottom of the sample. The reference points RP-1 and RP-2 are respectively selected for load and restraint application. The constraint between the bearing strip and the sample is defined using a tie, and the constraint between the reference point and the bearing strip is designated using a rigid body. A downward displacement was applied at RP-1 to load the specimen. Through running the model in ABAQUS, the reaction force is obtained at RP-1, and the maximum reaction force is substituted into

Equation (7) to calculate the tensile strength. The value of L in Equation (7) is equal to 1 mm, because the thickness of the 2D plane stress model in this study is set to 1 mm:

$$T = \frac{2000P}{\pi LD}$$

(7)

where T is the indirect tensile strength in MPa, P is the maximum reaction force indicated by the ABAQUS modeling in kilonewtons, L is the length of the CRM specimen in millimeters, and D is the diameter in millimeters.
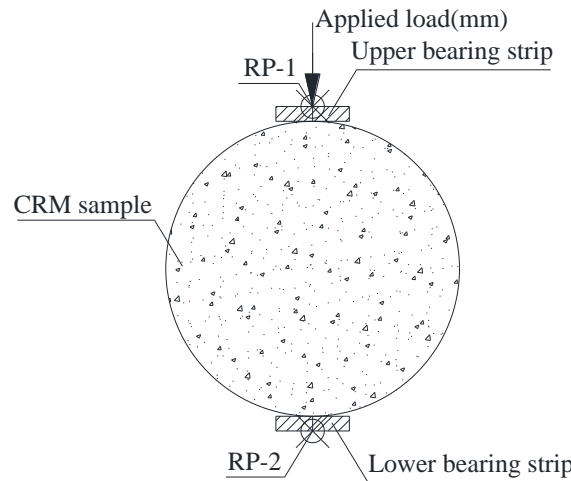

Figure 10. Schematic diagram of CRM specimen for indirect tensile test.

3.1.6. Simulation of Three-Point Flexural Test

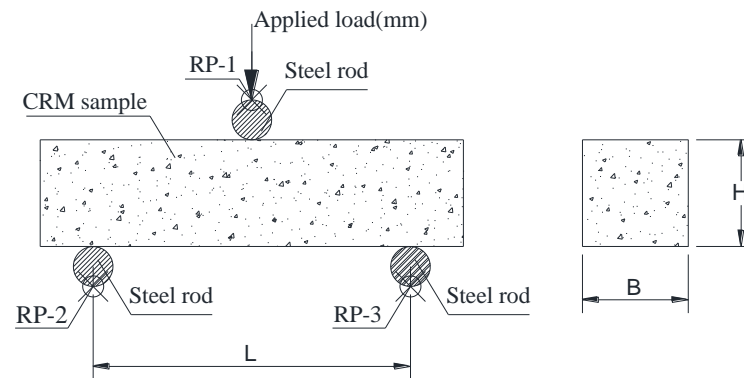Figure 11 presents the schematic diagram of the CRM specimen for modeling the three-point flexural test.

Figure 11. Schematic diagram of CRM specimen three-point flexural test.

The reference point RP-1 on the top of the steel rod, which is located in the middle of the specimen, is selected as the load application point. The reference points RP-2 and RP-2, which are located on the left and right steel rods, are used as constraint application points. The type of restraint between the steel bar and the specimen is designated as "tie", and the constraint type between the steel rod and its reference point is set to "rigid body". The value of B in Equation (8) is set to 1 mm:

$$S_f = \frac{3PL}{2BH^2}$$

(8)

where S_f is flexural strength in MPa, P is the total maximum load indicated by the testing machine, or the maximum reaction of RP-1 obtained from ABAQUS in Newton, L is the

span length of the CRM specimen in millimeters, B is the width in millimeters, and H is the height of the CRM specimen.

3.2. Numerical Analysis of Influencing Factors of Indirect Tensile Strength

In this section, the effects of the presence of the ITZ, the distribution of rubber aggregates, and the strength of the mortar matrix, regarding rubber particles as pores on the tensile strength of CRM, were investigated using the finite element method (FEM). The element type of FE mesh was set to 4-node plane stress (CPS4R), the thickness of all elements was set to 1 mm, and the global size of FE was set to 0.5 mm.

3.2.1. The Influence of the Presence of ITZ

A mesoscale model of the CRM containing an ITZ with a thickness of 0.05 mm was created to study its effect on the tensile strength of the CRM containing circular rubber particles with three sizes of 1.18–2.36 mm, 2–4 mm, and 6–8 mm. The strength of the ITZ in the CRM was set to 60% of the mortar phase (see Table 4), and then it was set to 100% of the mortar phase to ignore the presence of the ITZ. Then, the results of the tensile strength of the different CRM models were compared.

Table 5 shows the tensile strength of the 18 models. First, by comparing the results between the third and fourth columns, it indicates that changing the strength of the ITZ creates a slight decrease in the tensile strength. Figure 12 shows the strength reduction rate of CRMs with different rubber contents and sizes after the ITZ is considered. The strength reduction rate of the CRM due to the ITZ effect increases slightly as the rubber content increases from 6% to 18%. Since the maximum reduction in the tensile strength of the CRM is 0.99%, the presence of the ITZ can be ignored when studying the effect of rubber particles on the tensile strength of the CRM.

Table 5. Variation in tensile strength of CRM after ITZ is considered.

Rubber Content (%)	Rubber Size (mm)	Tensile Strength of CRM without ITZ (MPa)	Tensile Strength of CRM with ITZ (MPa)	Reduction Rate
6%		3.865	3.856	0.24%
12%	1.18–2.36 mm	3.534	3.511	0.67%
18%		3.227	3.195	0.99%
6%		3.928	3.923	0.12%
12%	2–4 mm	3.867	3.862	0.12%
18%		3.526	3.513	0.37%
6%		3.859	3.856	0.07%
12%	6–8 mm	3.714	3.710	0.11%
18%		3.580	3.575	0.16%

Figure 13 compares the area ratio of the ITZ to rubber particles in the CRM, showing that the area ratio of the ITZ is mainly related to rubber size. As the rubber size decreased from 6–8 mm to 1.18–2.36 mm, the area ratio of the ITZ increased from approximately 2.9% to 11%, suggesting that the use of smaller-sized rubber particles resulted in a larger ITZ area and a slightly greater reduction in tensile strength.
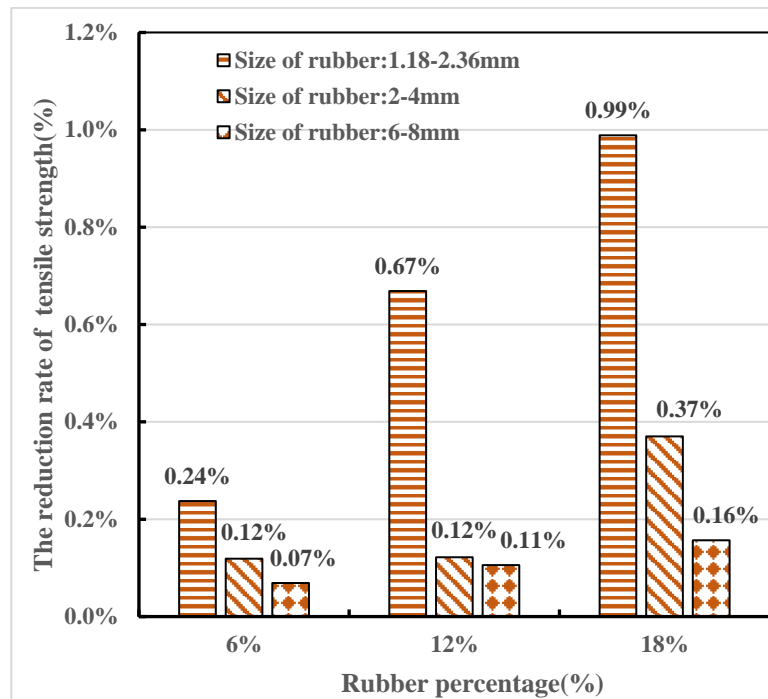
Figure 12. The tensile strength reduction rate of CRM after ITZ is considered.
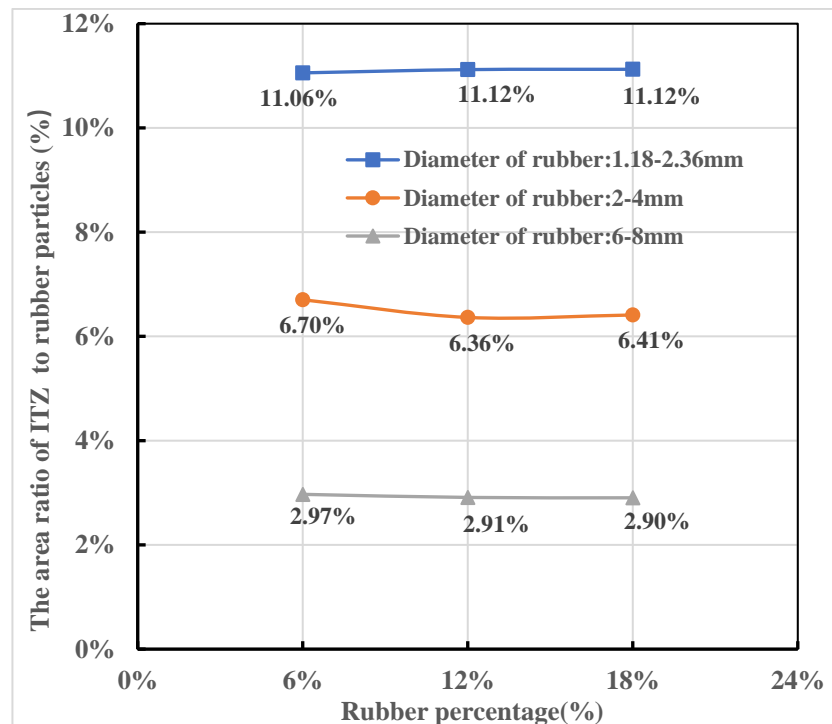

Figure 13. The area ratio of ITZ to rubber particle in CRM.

3.2.2. The Influence of Rubber Aggregate Distributions

A numerical simulation was conducted for six CRM specimens with different aggregate distributions but the same rubber content to evaluate the influence of the locations of rubber aggregates on the tensile strength of CRM. Different rubber particles sizes were tried, including sizes of 0.86 mm, 1.77 mm, 3 mm, 5 mm, and 7 mm. The rubber content of the CRM sample was set to 6% and 18%, and the shape of the rubber particle was simulated as a circle.

Table 6 compares the tensile strength of CRM specimens with the six distinct rubber aggregates and the two different rubber contents. Standard deviation was used to describe the stability of the tensile strength changes of the six CRM samples. The results indicate that rubber aggregate size affects the tensile strength, and the standard deviation of CRM samples containing smaller-sized rubber particles (such as 1.77 mm) is lower than that containing large sizes (such as 7 mm). To achieve the same rubber content, the number of small-sized rubber particles used will be much larger than the larger ones. Therefore, adding small-sized rubber particles into the mortar and fully mixing them makes the internal structure of the rubber mortar more uniform.

Table 6. The tensile strength of CRM 6 and CRM 18 with six kinds of aggregate distributions.

Sample	Rubber Particle Size(mm)				
	0.86	1.77	3	5	7
CRM6-1	3.83	3.89	3.92	3.92	3.81
CRM6-2	3.76	3.83	3.77	3.34	3.78
CRM6-3	3.76	3.76	3.75	3.82	4.11
CRM6-4	3.76	3.84	3.78	3.88	3.75
CRM6-5	3.80	3.71	3.48	3.37	3.10
CRM6-6	3.76	3.67	3.76	4.02	4.00
Average(MPa)	3.78	3.78	3.74	3.73	3.76
Standard Deviation(MPa)	0.03	0.08	0.13	0.27	0.32
CRM18-1	3.29	3.34	3.36	3.71	3.75
CRM18-2	3.31	3.21	3.27	3.02	2.61
CRM18-3	3.28	3.22	3.18	3.08	2.52
CRM18-4	3.35	3.17	3.37	3.18	3.29
CRM18-5	3.31	3.27	3.21	2.92	2.74
CRM18-6	3.34	3.15	3.43	3.60	3.89
Average(MPa)	3.32	3.23	3.30	3.25	3.13
Standard Deviation(MPa)	0.02	0.06	0.09	0.30	0.54

Figure 14 presents the final damage mode of CRM specimens with 7 mm rubber particles, showing that tensile and compressive damage mainly formed in the CRM specimen along its diameter.

3.2.3. The Influence of Mortar Matrix Strength

The compressive strength of the control mortar is 66.83 MPa (see Table 4), which was multiplied by a number less than 1 to obtain the four strengths including 20 MPa, 30 MPa, 40 MPa, and 50 MPa. These four control mortars were respectively modeled with 2–4 mm rubber particles to form rubber mortar. The indirect tensile strength and Young's modulus of the four control mortars were obtained similarly. The purpose was to investigate whether the rate of decrease in the tensile strength is related to the strength of the control mortar. The shape of rubber particles in CRM was treated as a circle-derived polygon. The ratio of the indirect tensile strength between the CRM and the control mortar is shown in Figure 15, indicating that the strength reduction rate is not affected by the strength of the control mortar, but is related to the rubber content.

3.2.4. The Influence of Treating Rubber Particles as Pores

Since the rigidity of rubber is much lower than that of sand, replacing sand with rubber particles is similar to adding the same number of pores to mortar. Therefore, the feasibility of equating rubber particles with pores is studied in this section. CRM models mixed with 2–4 mm rubber particles were first created, and then their rubber particles were replaced by pores to generate reference specimens. The results of these two types of samples are shown in Figure 16, indicating that rubber particles can be regarded as pores when predicting the indirect tensile strength of CRM, and the difference is negligible.
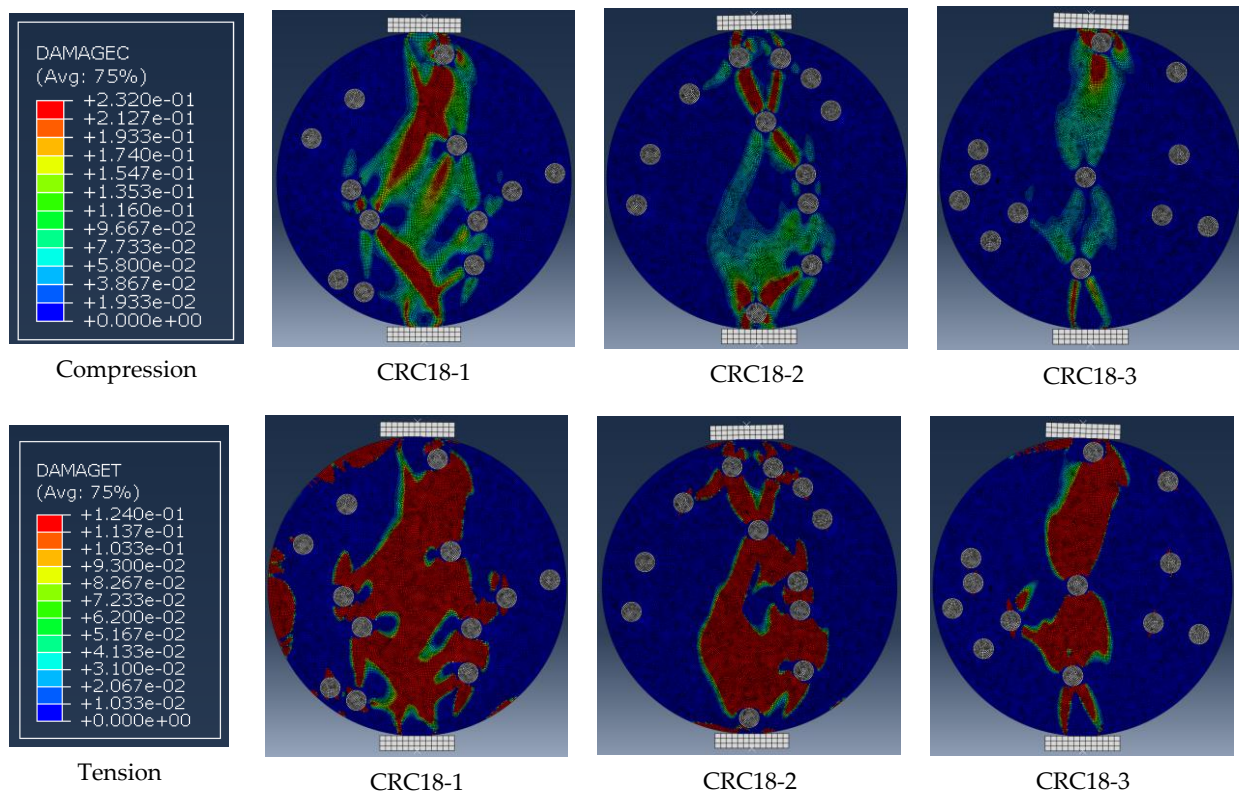
Figure 14. Compressive and tensile damage of three CRM 18 specimens added with 7 mm circular rubber particles.

Figure 17 shows the damage pattern of the reference sample with pores and the corresponding CRM sample, which indicates that the rubber particles and pores have the same effect on the strength and failure mode. Therefore, it can be concluded that the stress concentration caused by the incorporation of rubber particles is one of the reasons for the decrease in the strength of the rubber mortar. Ordinary mortar can be regarded as a continuous material. The added rubber particles increase the irregularity of the internal structure of the CRM and produce weak zones, which interrupts the stress flow and causes higher concentration stress at the location of the rubber particles. The area around the rubber particles cracks at low-stress levels, and then the ultimate strength of the rubber mortar decreases correspondingly.

To consider the effect of the different distribution of rubber particles on the tensile strength of CRM, six pore-based CRM models were generated for each mixture to calculate the tensile strength, as shown in Table 7.

3.2.5. Numerical Analysis Summary

The analysis of the above four influencing factors shows that the presence of ITZ on the tensile strength of CRM is negligible. The tensile strengths of CRM samples with the same rubber content but different rubber particle distributions are different, and the variation range increases with the increase in rubber particle size.

The strength of the control mortar does not affect the tensile strength reduction rate of CRM. Rubber particles can be idealized as pores to create mesoscale models of CRM samples.
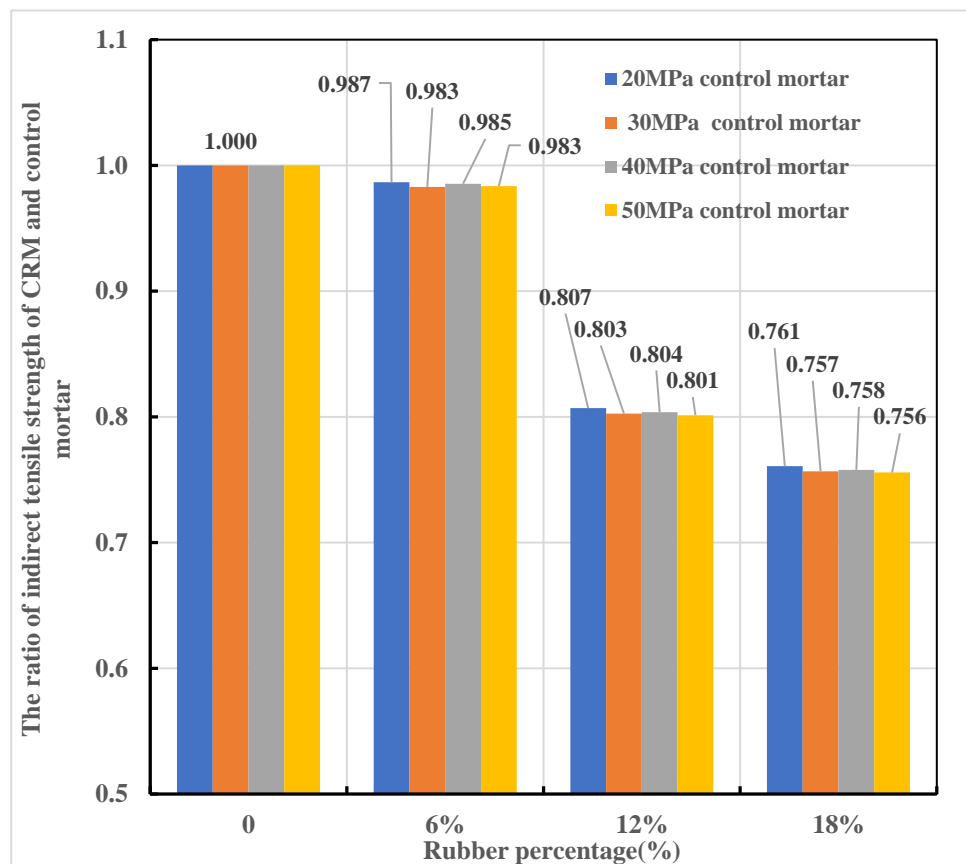
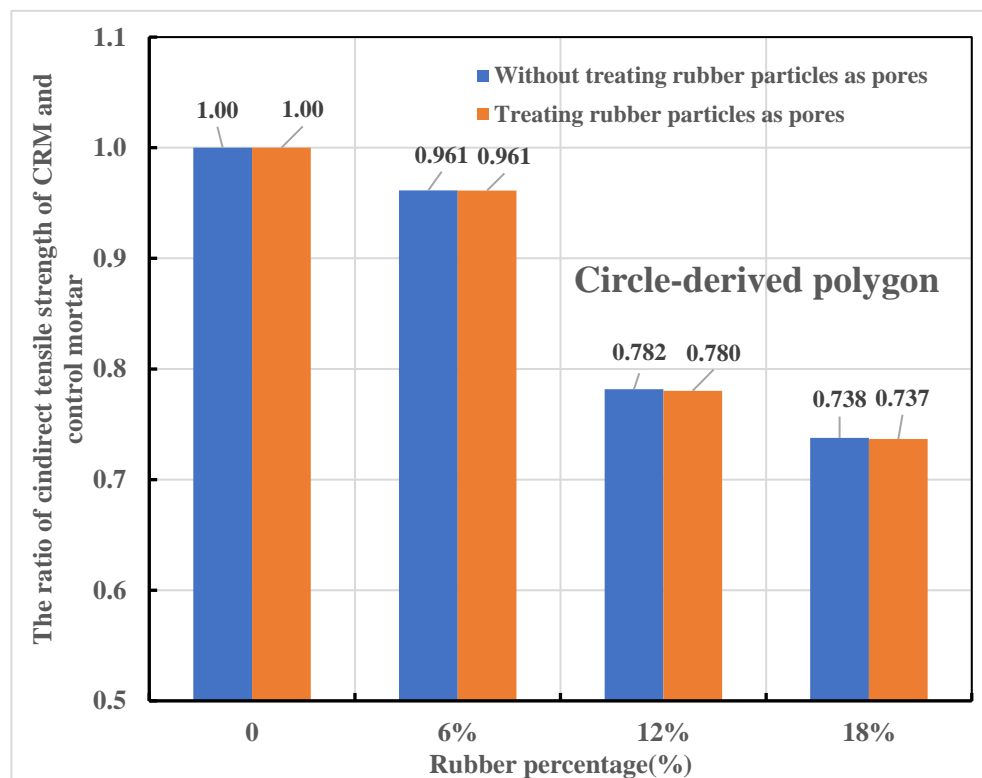**Figure 15.** Changes in indirect tensile strength of CRM with different rubber contents.

Figure 16. Changes in the indirect tensile strength of CRM models after treating rubber particles as pores.
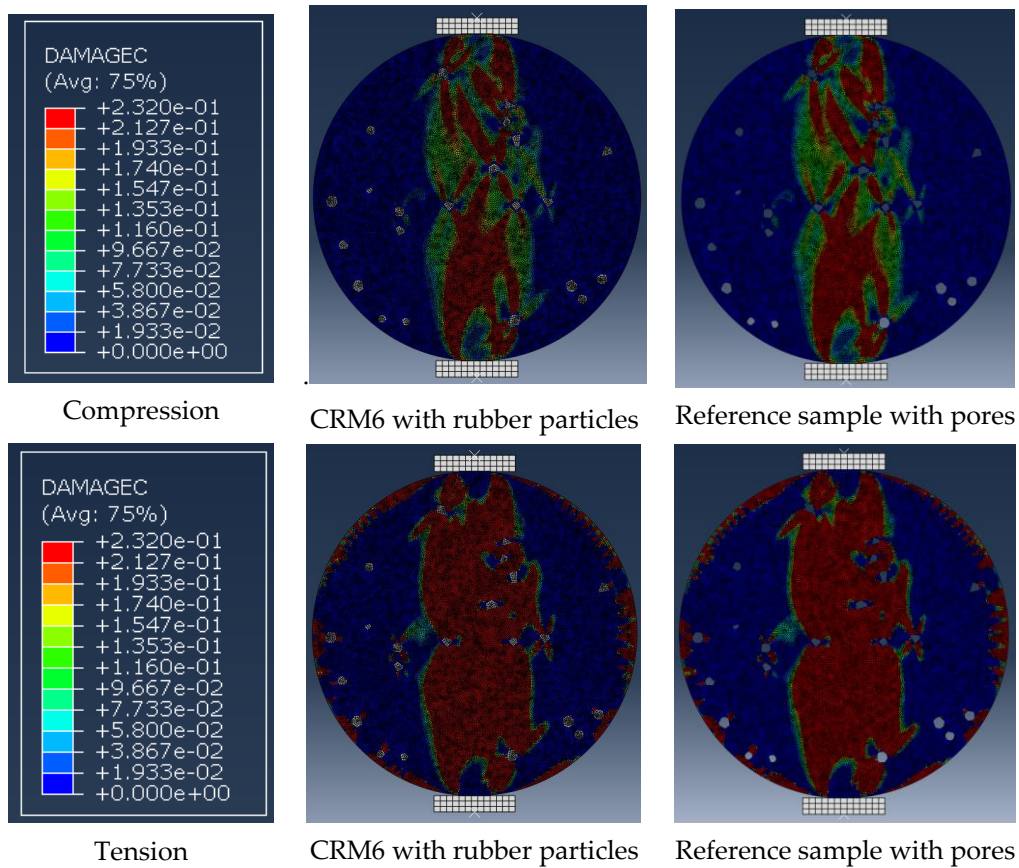
Figure 17. Comparison of damage modes between CRM specimens and reference specimens with pores.

Table 7. The tensile strength of CRM obtained by numerical simulation.

Mix	Rubber Content (%)	Calculated Results (MPa)	Average (MPa)	Average Strength Ratio of CRM and Control Mix
Control	0%	4.08	4.08	1
CRM6-1		3.92		
CRM6-2		3.57		
CRM6-3	6%	3.81	3.77	0.92
CRM6-4		3.84		
CRM6-5		3.81		
CRM6-6		3.69		
CRM12-1		3.19		
CRM12-2		3.48		
CRM12-3	12%	3.50	3.47	0.85
CRM12-4		3.65		
CRM12-5		3.62		
CRM12-6		3.38		
CRM18-1		3.01		
CRM18-2		3.24		
CRM18-3	18%	3.35	3.23	0.79
CRM18-4		3.46		
CRM18-5		3.33		
CRM18-6		3.02		

4. Mesoscale Model Applications and Validation

In this section, two groups of experimental tests have been conducted to determine the tensile strength and flexural strength of CRM, respectively. The results agreed well with the numerical models.

4.1. A Pore-Based Mesoscale Model for Predicting the Tensile Strength of CRM

Onuaguluchi and Panesar (2014) and Uygunoğlu and Topçu (2010) concluded that the porosity of rubber concrete will increase slightly as the content of rubber particles increases [6,40]. Microstructure experiments showed that there are more pores gathered near the rubber particles, and the density of the ITZ is lower than that of ordinary concrete [37]. Yu and Zhu (2016) replaced sand in the normal mortar with rubber particles at three levels of 17%, 33%, and 50% by weight and tested the porosity of CRM samples [14]. The results showed that as the rubber content increased from 17% to 50%, the porosity of the CRM containing 2–4 mm rubber particles increased from 16.27% to 18.94%.

The effect of rubber on the porosity of CRM was considered in this analysis. The apparent volume of permeable voids in the CRM was tested experimentally following ASTM C 642-06 (1997) [41]. Three cubes with a size of 50 mm were prepared for CRM with rubber contents of 0–18%. Sand accounts for 44.27% of the total volume of the control mix (see Table 1), and the volume ratio of rubber particles to the CRM sample can be calculated by multiplying the sand content by the rubber replacement rate. For CRM added with 2–4 mm rubber particles, the volume ratios of rubber to sample in CRM6, CRM12, and CRM18 were 2.66%, 5.31%, and 7.97%, respectively. The best fit curve between porosity and rubber content is shown in Figure 18. The equation of the curve is described as:

$$P_v = 0.2072\rho_s + 0.226 \tag{9}$$

where P_v is the porosity of CRM, and ρ_s is the rubber content over the total volume of the sample.
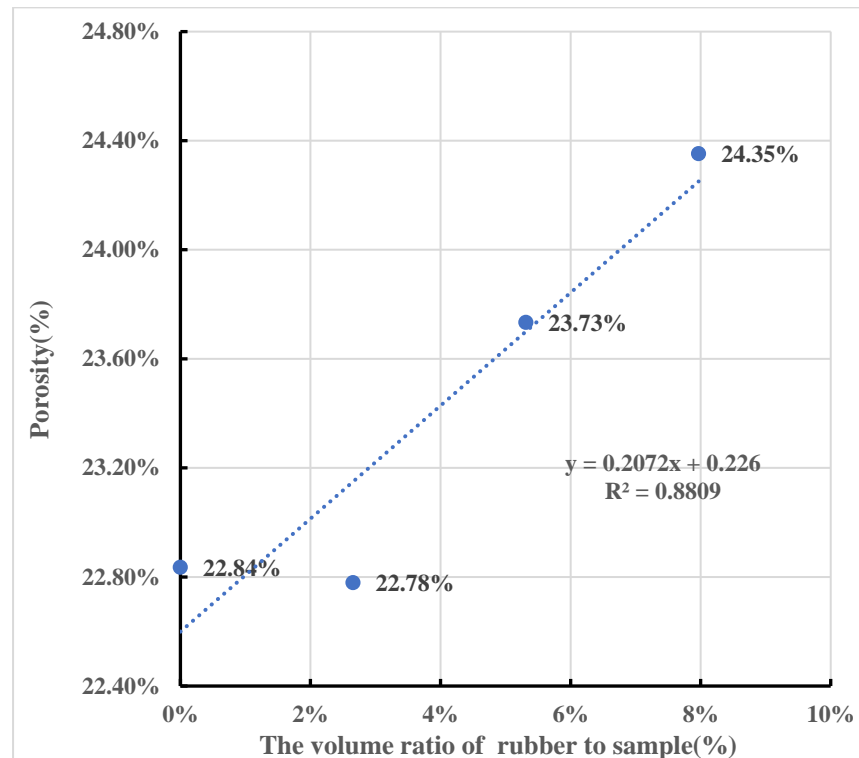

Figure 18. The effect of rubber content on the porosity of CRM.

In the indirect tensile tests, the cylindrical specimen is loaded radially along its diameter, as shown in Figure 19. Three samples for each mixture were cast to test the indirect tensile strength of CRM, and their average was taken as the experimental value. The results of CRM samples are listed in Table 8.

Figure 19. Failure modes of CRM12 specimens.

Table 8. Test results of indirect tensile strength.

Rubber Content	0%	6%	12%	18%
Indirect tensile strength (MPa)	4.44	3.76	2.92	2.60
	3.52	3.83	3.29	2.81
	3.98	3.75	2.87	2.65
Average (MPa)	3.98	3.78	3.03	2.69
Standard deviation (MPa)	0.38	0.04	0.19	0.09

Based on the numerical results from Table 7 in Section 3.2.4, the best-fitting curve of the average tensile strength of CRM and rubber content is shown in Figure 20. Equation (9) shows that the porosity of the CRM is larger than the control mortar. To consider the effect of the increased porosity, the equation of the curve should be modified as

$$R_T = 6.359(\rho_t + \Delta P_v)^2 - 3.1256\,(\rho_t + \Delta P_v) + 1.0008 \tag{10}$$

where R_T is the ratio of the indirect tensile strength of CRM over the control mortar, ρ_t is the volume ratio of rubber to the sample, the values of ρ_t of CRM6, CRM12, and CRM 18 are listed in Table 9, and ΔP_v is the increased porosity of CRM over the control mortar, which can be calculated based on Equation (9).

Table 9 provides detailed calculations of porosity in CRM. Calculated values of tensile strength for CRMs with three rubber contents were obtained using Equation (10). The comparison between the predicted formula of Equation (10) and test results are compared in Figure 21. The errors of CRM6, CRM12, and CRM18 are −2.08%, 11.29%, and 15.21%, respectively. The maximum absolute value of the difference between the simulated value and the experimental value is 0.41 Mpa, which is acceptable.
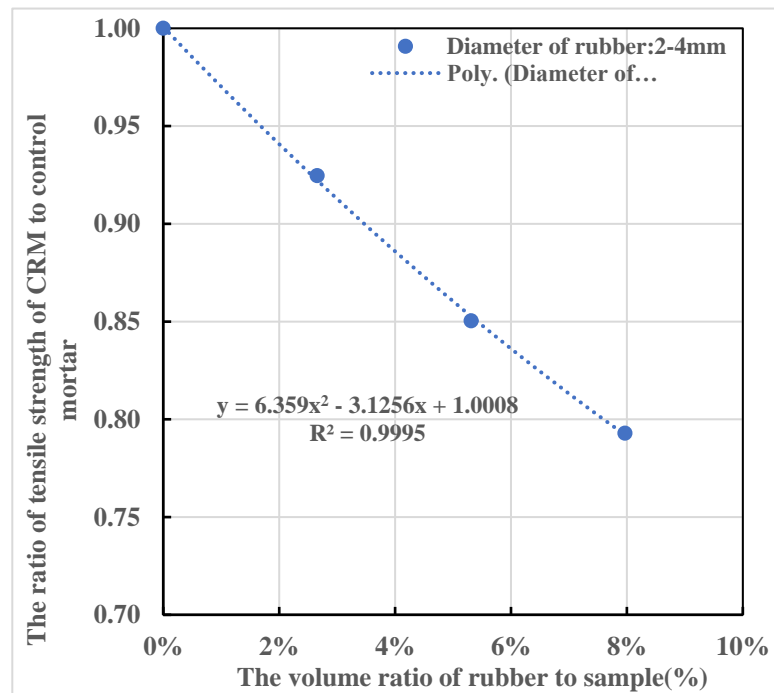
Figure 20. The best-fitting curve of indirect tensile strength and rubber content.

Table 9. Increased porosity of the CRM caused by the use of rubber particles.

Mix	Rubber Content (%)	The Volume Ratio of Rubber and the Sample	Porosity of CRM	Increase in Porosity of CRM	Sum of Increased Porosity and Rubber Percentage
Control	0	0.00%	22.60%	0.00%	0.00%
CRM6	6%	2.66%	23.15%	0.55%	3.21%
CRM12	12%	5.31%	23.70%	1.10%	6.41%
CRM18	18%	7.97%	24.25%	1.65%	9.62%

4.2. A Pore-Based Mesoscale Model for Predicting the Flexural Strength of CRM

A three-point flexural test was performed to investigate the effect of adding rubber particles on the flexural strength of the CRM. Cracks mainly occurred in the middle of the specimen (Figure 22), and the test results of the flexural strength of CRM samples are listed in Table 10.

Table 10. Test results of flexural strength.

Rubber Content	0%	6%	12%	18%
	7.65	8.33	5.89	6.01
Flexural strength (MPa)	7.92	6.73	6.06	5.84
	8.52	7.27	6.73	5.32
Average (MPa)	8.03	7.45	6.23	5.72
Standard deviation (MPa)	0.37	0.66	0.36	0.30

The method described in Section 4.1 was also used to develop a pore-based model to simulate the flexural strength test of the CRM. A 2D sample of CRM12 with rubber particles is shown in Figure 23; these rubber particles are replaced by the same number of pores to generate a pore-based CRM model, as shown in Figure 24. Six models were created for each CRM mixture to obtain theoretical values of flexural strength, and the results are shown in Table 11. In the numerical analysis, the area in which the tensile damage occurs is located at the bottom of the specimen, as shown in Figure 25.
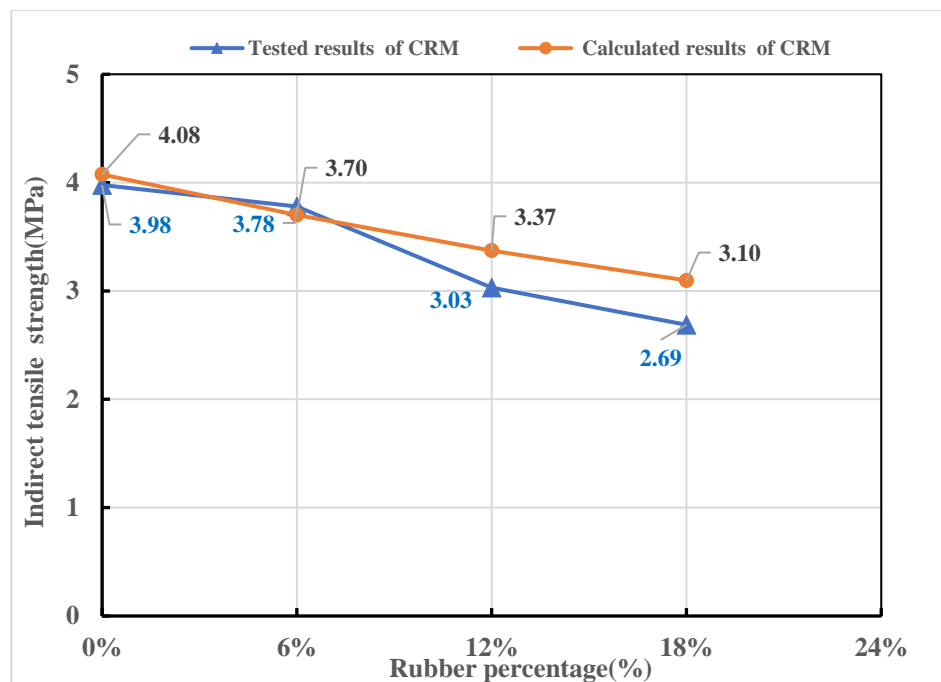
Figure 21. Comparison of results obtained from experiment and mesoscale simulation.
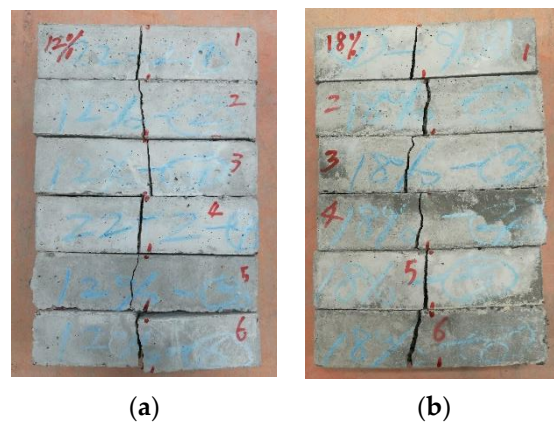

(a) (b)

Figure 22. Failure modes of CRM specimens. (**a**) Sample with 12% rubber content. (**b**) Sample with 18% rubber content.
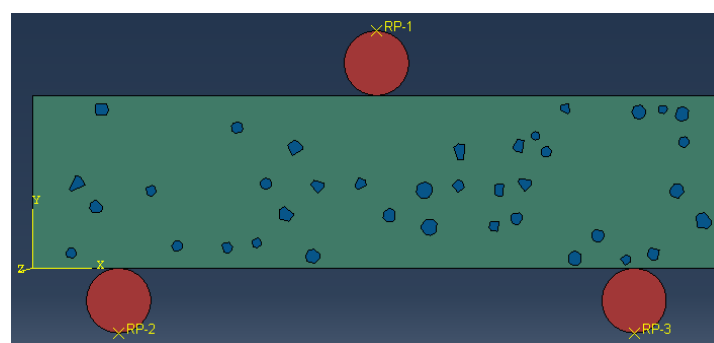

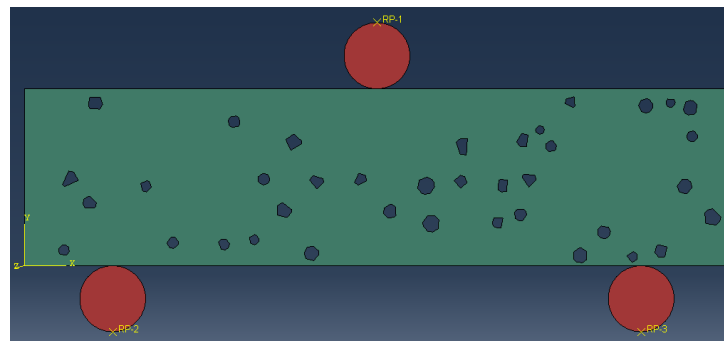**Figure 23.** Rubber particles in a 2D CRM6 sample.

Figure 24. Pore-based mesoscale model of the 2D CRM12 sample.

Table 11. The flexural strength of CRM obtained by numerical simulation.

Mix	Rubber Content (%)	Calculated Results (MPa)	Average (Mpa)	Average Strength Ratio of CRM and Control Mix
Control	0%	7.93	7.93	1
CRM6-1		6.85		
CRM6-2		6.42		
CRM6-3		6.65		
CRM6-4	6%	7.45	6.93	0.87
CRM6-5		6.85		
CRM6-6		7.37		
CRM12-1		6.70		
CRM12-2		5.69		
CRM12-3		6.58		
CRM12-4	12%	6.88	6.51	0.82
CRM12-5		6.28		
CRM12-6		6.96		
CRM18-1		6.25		
CRM18-2		5.55		
CRM18-3		6.36		
CRM18-4	18%	6.51	6.20	0.78
CRM18-5		6.08		
CRM18-6		6.44		
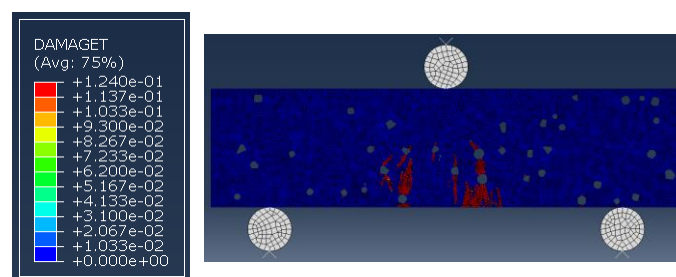
Figure 25. Tensile damage of CRM 12 specimens.

Figure 26 presents the best-fitting curve of the flexural strength reduction rate and the rubber content. To consider the effect of the increased porosity, the equation of the curve is expressed as:

$$R_T = -534.17(\rho_t + \Delta P_v)^3 + 94.328(\rho_t + \Delta P_v)^2 - 6.8641(\rho_t + \Delta P_v) + 1 \tag{11}$$

where R_T is the ratio of the flexural strength of the CRM and the control mortar, ρ_t is the volume ratio of rubber to the sample, and ΔP_v is the increased porosity of CRM over the control mortar, which can be calculated based on Equation (9).
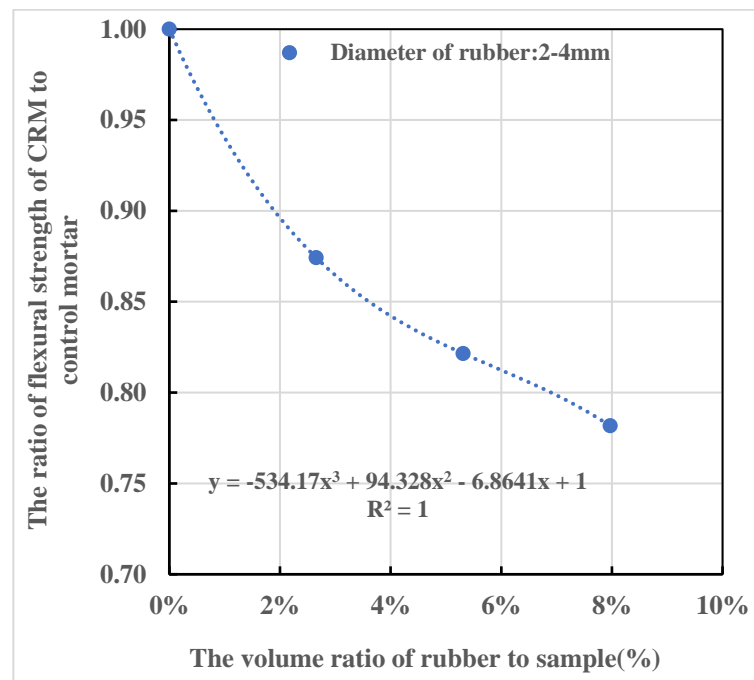

Figure 26. The best-fitting curve of flexural strength and rubber particle content.

Calculated values of flexural strength for CRMs with three rubber contents were obtained using Equation (11).

Figure 27 compares the results of experimental testing and the predicted formula of Equation (11), indicating that an increase in rubber content leads to a decrease in flexural strength. When the rubber content was increased from 0% to 6%, the strength reduction rate was 14%. Then, every 6% increase in rubber content results in a 5–6% decrease in flexural strength. The deviations of the experimental and simulated values for CRM6, CRM12, and CRM18 are −8.49%, 2.71%, and 2.13%, respectively, all within the acceptable range.
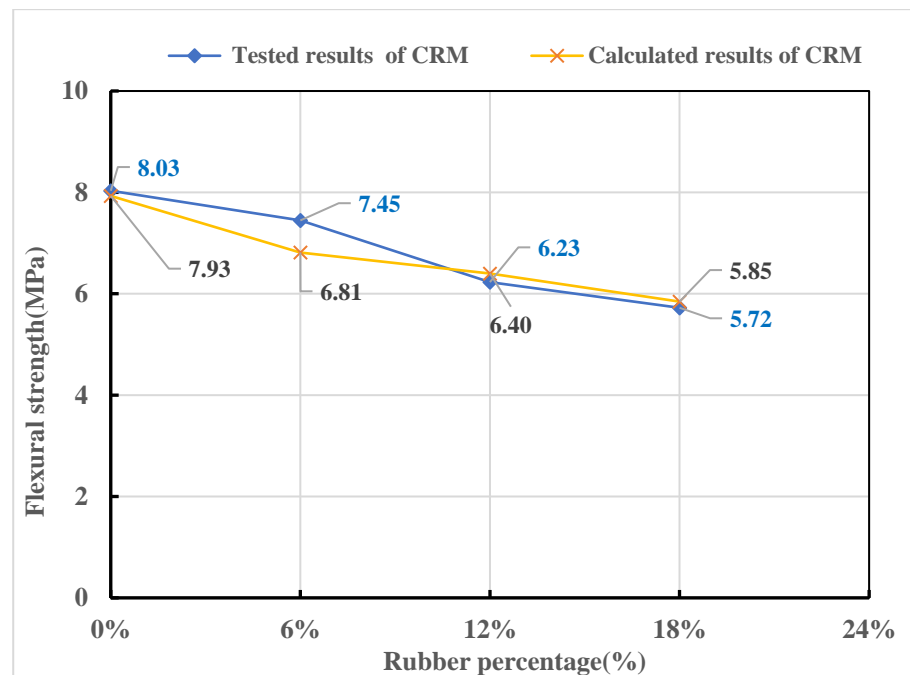
Figure 27. Comparison of experimental and calculated values of flexural strength of CRM.

5. Conclusions

Experimental tests were conducted to measure the indirect tensile and flexural strengths of CRMs with different rubber contents. The effects of changing the ITZ strength, the rubber aggregate distribution, and the mortar matrix regarding rubber particles as pores were studied through numerical analysis. A pore-based mesoscale model was presented to predict the tensile and flexural strength of CRM, and the results match well with experimental results. The conclusions of the numerical simulation and laboratory test results are as follows:

(1) Rubber content is a controlling factor that determines the strength of CRM. For every 6% increase in the rubber content, the tensile strength and flexural strength of the rubber mortar decreased by around 8% and 9%, respectively. The influence of the shape of the rubber particles on the strength of the CRM can be neglected.

(2) Rubber particle size affects the strength variation of CRM. The use of smaller-sized rubber particles tends to result in a more uniform internal structure of the CRM and a smaller range of strength variations for the CRM samples. As the size of the rubber particles increases, the heterogeneity of the rubber particle distribution between the different CRM samples also increases, resulting in a wider range of their strength variation.

(3) The influence of the ITZ on the strength of CRM is 0.99%, which can be ignored. The presence of the ITZ has a greater effect on CRM samples with smaller rubber particles, resulting in a slightly higher rate of strength reduction. As the rubber size increases from 1.18–2.36 mm to 6–8 mm, the effect of the ITZ on tensile strength decreases from 0.99% to 0.16%.

(4) The use of rubber particles decreases the tensile and flexural strength of CRM. Rubber particles and pore areas are weak locations, and microcracks occur near them at low-stress levels, resulting in a reduction in strength. The addition of rubber particles increases the air content of CRM compared to the control mixture; the porosity of the CRM increases by 1.15% for every 6% increase in rubber content. The effect of increased air content on the tensile and flexural strength of CRM needs to be considered. The failure mode of the CRM model in a numerical simulation shows that tensile and compressive damage typically occurs in and around the area in which the rubber particles and voids are located.

References

1. Zhu, H.; Thong-On, N.; Zhang, X. Adding crumb rubber into exterior wall materials. *Waste Manag. Res.* **2002**, *20*, 407–413. [CrossRef] [PubMed]
2. Wongsa, A.; Sata, V.; Nematollahi, B.; Sanjayan, J.; Chindaprasirt, P. Mechanical and thermal properties of lightweight geopolymer mortar incorporating crumb rubber. *J. Clean. Prod.* **2018**, *195*, 1069–1080. [CrossRef]
3. Di Mundo, R.; Seara-Paz, S.; González-Fonteboa, B.; Notarnicola, M. Masonry and render mortars with tyre rubber as aggregate: Fresh state rheology and hardened state performances. *Constr. Build. Mater.* **2020**, *245*, 118359. [CrossRef]
4. de Souza Kazmierczak, C.; Schneider, S.D.; Aguilera, O.; Albert, C.C.; Mancio, M. Rendering mortars with crumb rubber: Mechanical strength, thermal and fire properties and durability behaviour. *Constr. Build. Mater.* **2020**, *253*, 119002. [CrossRef]
5. Li, J.; Saberian, M.; Nguyen, B.T. Effect of crumb rubber on the mechanical properties of crushed recycled pavement materials. *J. Environ. Manag.* **2018**, *218*, 291–299. [CrossRef]
6. Uygunoğlu, T.; Topçu, İ.B. The role of scrap rubber particles on the drying shrinkage and mechanical properties of self-consolidating mortars. *Constr. Build. Mater.* **2010**, *24*, 1141–1150. [CrossRef]
7. Eltayeb, E.; Ma, X.; Zhuge, Y.; Youssf, O.; Mills, J. Influence of rubber particles on the properties of foam concrete. *J. Build. Eng.* **2020**, *30*, 101217. [CrossRef]
8. Eltayeb, E.; Ma, X.; Zhuge, Y.; Xiao, J.; Youssf, O. Composite walls Composed of profiled steel skin and foam rubberized concrete subjected to eccentric compressions. *J. Build. Eng.* **2022**, *46*, 103715. [CrossRef]
9. Eltayeb, E.; Ma, X.; Zhuge, Y.; Youssf, O.; Mill, J.; Xiao, J. Structural behaviour of composite panels made of profiled steel sheets and foam rubberised concrete under monotonic and cyclic shearing loads. *Thin-Walled Struct.* **2020**, *151*, 10672. [CrossRef]
10. Eltayeb, E.; Ma, X.; Zhuge, Y.; Youssf, O.; Mill, J.; Xiao, J. Structural performance of composite panels made of profiled steel skins and foam rubberised concrete under axial compressive loads. *Eng. Struct.* **2020**, *211*, 110448. [CrossRef]
11. Marques, A.C.; Akasaki, J.L.; Trigo, A.P.M.; Marques, M.L. Influence of the surface treatment of tire rubber residues added in mortars. *Rev. IBRACON Estrut. Mater.* **2008**, *1*, 113–120. [CrossRef]
12. Correia, S.L.; Partala, T.; Loch, F.C.; Segadães, A.M. Factorial design used to model the compressive strength of mortars containing recycled rubber. *Compos. Struct.* **2010**, *92*, 2047–2051. [CrossRef]
13. Song, W.-J.; Qiao, W.-G.; Yang, X.-X.; Lin, D.-G.; Li, Y.-Z. Mechanical properties and constitutive equations of crumb rubber mortars. *Constr. Build. Mater.* **2018**, *172*, 660–669. [CrossRef]
14. Yu, Y.; Zhu, H. Influence of Rubber Size on Properties of Crumb Rubber Mortars. *Materials* **2016**, *9*, 527. [CrossRef] [PubMed]
15. Turatsinze, A.; Granju, J.-L.; Bonnet, S. Positive synergy between steel-fibres and rubber aggregates: Effect on the resistance of cement-based mortars to shrinkage cracking. *Cem. Concr. Res.* **2006**, *36*, 1692–1697. [CrossRef]
16. Turki, M.; Bretagne, E.; Rouis, M.J.; Quéneudec, M. Microstructure, physical and mechanical properties of mortar–rubber aggregates mixtures. *Constr. Build. Mater.* **2009**, *23*, 2715–2722. [CrossRef]
17. Rodrigues, E.A.; Manzoli, O.L.; Bitencourt, L.A.G., Jr.; Bittencourt, T.N. 2D mesoscale model for concrete based on the use of interface element with a high aspect ratio. *Int. J. Solids Struct.* **2016**, *94–95*, 112–124. [CrossRef]
18. Wang, X.; Zhang, M.; Jivkov, A.P. Computational technology for analysis of 3D meso-structure effects on damage and failure of concrete. *Int. J. Solids Struct.* **2016**, *80*, 310–333. [CrossRef]
19. Forti, T.; Batistela, G.; Forti, N.; Vianna, N. 3D Mesoscale Finite Element Modelling of Concrete under Uniaxial Loadings. *Materials* **2020**, *13*, 4585. [CrossRef]
20. Chen, H.; Xu, B.; Mo, Y.L.; Zhou, T. Behavior of meso-scale heterogeneous concrete under uniaxial tensile and compressive loadings. *Constr. Build. Mater.* **2018**, *178*, 418–431. [CrossRef]
21. Sheng, P.; Zhang, J.; Ji, Z. An advanced 3D modeling method for concrete-like particle-reinforced composites with high volume fraction of randomly distributed particles. *Compos. Sci. Technol.* **2016**, *134*, 26–35. [CrossRef]
22. Guo, R.; Ren, H.; Zhang, L.; Long, Z.; Jiang, X.; Wu, X.; Wang, H. Direct dynamic tensile study of concrete materials based on mesoscale model. *Int. J. Impact Eng.* **2020**, *143*, 103598. [CrossRef]

23. Zhou, R.; Song, Z.; Lu, Y. 3D mesoscale finite element modelling of concrete. *Comput. Struct.* **2017**, *192*, 96–113. [CrossRef]
24. Huang, Y.J.; Yang, Z.J.; Chen, X.W.; Liu, G.H. Monte Carlo simulations of meso-scale dynamic compressive behavior of concrete based on X-ray computed tomography images. *Int. J. Impact Eng.* **2016**, *97*, 102–115. [CrossRef]
25. Duarte, A.P.C.; Silva, B.A.; Silvestre, N.; De Brito, J.; Júlio, E. Mechanical characterization of rubberized concrete using an image-processing/XFEM coupled procedure. *Compos. Part B Eng.* **2015**, *78*, 214–226. [CrossRef]
26. Duarte, A.P.C.; Silvestre, N.; de Brito, J.; Júlio, E. Numerical study of the compressive mechanical behaviour of rubberized concrete using the eXtended Finite Element Method (XFEM). *Compos. Struct.* **2017**, *179*, 132–145. [CrossRef]
27. Li, X.; Chen, X.; Jivkov, A.P.; Zhang, J. 3D mesoscale modeling and fracture property study of rubberized self-compacting concrete based on uniaxial tension test. *Theor. Appl. Fract. Mech.* **2019**, *104*, 102363. [CrossRef]
28. Diao, H.; Wang, X.; Cui, Y.; Han, S.; Qi, C. Analysis of Rubberized Self-Compacting Concrete under Uniaxial Tension by 3D Mesoscale Models. *Adv. Civ. Eng.* **2020**, *2020*, 8854730. [CrossRef]
29. *AS 1012.8.1*; AS1012.8.1:2014 Methods of Testing Concrete Method 8.1: Method for Making and Curing Concrete—Compression and Indirect Tensile Test Specimens. Standards Australia: Sydney, Australia, 2014.
30. *ASTM: C-348-20*; Standard Test Method for Flexural Strength of Hydraulic-Cement Mortars. ASTM International: West Conshohocken, PA, USA, 1999. [CrossRef]
31. *AS 1012.10*; Australian Standard 1012.10: Methods of Testing Concrete-Determination of Indirect Tensile Strength of Concrete Cylinders ('Brazil' or Splitting Test). Standards Australia: Sydney, Australia, 2000.
32. Chen, H.; Li, D.; Ma, X.; Zhong, Z.; Abd-Elaal, E.-S. Mesoscale analysis of rubber particle effect on young's modulus and creep behaviour of crumb rubber concrete. *Int. J. Mech. Mater. Des.* **2021**, *17*, 659–678. [CrossRef]
33. Kim, S.-M.; Al-Rub, R.K.A. Meso-scale computational modeling of the plastic-damage response of cementitious composites. *Cem. Concr. Res.* **2011**, *41*, 339–358. [CrossRef]
34. Scrivener, K.L.; Crumbie, A.K.; Laugesen, P. The Interfacial Transition Zone (ITZ) Between Cement Paste and Aggregate in Concrete. *Interface Sci.* **2004**, *12*, 411–421. [CrossRef]
35. D Systèmes. Analysis User's Guide: Volume III: Materials. In *ABAQUS 6.14 Analysis User's Guide 2014*; Abaqus Analysis, Dassault Systems: Boston, MA, USA, 2014; Volume III, p. 294.
36. Birtel, V.; Mark, P. Parameterised Finite Element Modelling of RC Beam Shear Failure. In Proceedings of the 2006 ABAQUS Users' Conference, Boston, MA, USA, 23–25 May 2006; pp. 95–108.
37. Wang, J.; Guo, Z.; Yuan, Q.; Zhang, P.; Fang, H. Effects of ages on the ITZ microstructure of crumb rubber concrete. *Constr. Build. Mater.* **2020**, *254*, 119329. [CrossRef]
38. Huang, Y.; Yang, Z.; Ren, W.; Liu, G.; Zhang, C. 3D meso-scale fracture modelling and validation of concrete based on in-situ X-ray Computed Tomography images using damage plasticity model. *Int. J. Solids Struct.* **2015**, *67–68*, 340–352. [CrossRef]
39. Xiao, J.; Li, W.; Corr, D.J.; Shah, S.P. Effects of interfacial transition zones on the stress–strain behavior of modeled recycled aggregate concrete. *Cem. Concr. Res.* **2013**, *52*, 82–99. [CrossRef]
40. Onuaguluchi, O.; Panesar, D.K. Hardened properties of concrete mixtures containing pre-coated crumb rubber and silica fume. *J. Clean. Prod.* **2014**, *82*, 125–131. [CrossRef]
41. *ASTM C 642-06*; Standard Test Method for Density, Absorption, and Voids in Hardened Concrete. ASTM International: West Conshohocken, PA, USA, 1997.